AGU PUBLICATIONS

Paleoceanography

CURRENTS

10.1002/2014PA002621

Key Points:
- Boron proxies document surface ocean acidification during the PETM
- Acidification was rapid and sustained, requiring prolonged carbon release
- Magnitude of acidification is at high end of estimates for PETM emissions

Supporting Information:
- Readme
- Text S1
- Table S1
- Table S2
- Figure S1
- Figure S2
- Figure S3
- Figure S4
- Figure S5

Correspondence to:
D. E. Penman,
dpenman@ucsc.edu

Citation:
Penman, D. E., B. Hönisch, R. E. Zeebe, E. Thomas, and J. C. Zachos (2014), Rapid and sustained surface ocean acidification during the Paleocene-Eocene Thermal Maximum, *Paleoceanography*, *29*, doi:10.1002/2014PA002621.

Received 28 JAN 2014
Accepted 16 APR 2014
Accepted article online 22 APR 2014

Rapid and sustained surface ocean acidification during the Paleocene-Eocene Thermal Maximum

Donald E. Penman[1], Bärbel Hönisch[2], Richard E. Zeebe[3], Ellen Thomas[4,5], and James C. Zachos[1]

[1]University of California, Santa Cruz, California, USA, [2]Department of Earth and Environmental Sciences, Lamont-Doherty Earth Observatory of Columbia University, Palisades, New York, USA, [3]University of Hawai'i at Mānoa, Honolulu, Hawaii, USA, [4]Yale University, New Haven, Connecticut, USA, [5]Wesleyan University, Middletown, Connecticut, USA

Abstract The Paleocene-Eocene Thermal Maximum (PETM) has been associated with the release of several thousands of petagrams of carbon (Pg C) as methane and/or carbon dioxide into the ocean-atmosphere system within ~10 kyr, on the basis of the co-occurrence of a carbon isotope excursion (CIE), widespread dissolution of deep sea carbonates, and global warming. In theory, this rapid carbon release should have severely acidified the surface ocean, though no geochemical evidence has yet been presented. Using boron-based proxies for surface ocean carbonate chemistry, we present the first observational evidence for a drop in the pH of surface and thermocline seawater during the PETM. Planktic foraminifers from a drill site in the North Pacific (Ocean Drilling Program Site 1209) show a ~0.8‰ decrease in boron isotopic composition ($\delta^{11}B$) at the onset of the event, along with a 30–40% reduction in shell B/Ca. Similar trends in $\delta^{11}B$ are present in two lower-resolution records from the South Atlantic and Equatorial Pacific. These observations are consistent with significant, global acidification of the surface ocean lasting at least 70 kyr and requiring sustained carbon release. The anomalies in the B records are consistent with an initial surface pH drop of ~0.3 units, at the upper range of model-based estimates of acidification.

1. Introduction

The Paleocene-Eocene Thermal Maximum (~56 million years, Ma) is marked by a 3–4‰ decrease in the carbon isotopic composition ($\delta^{13}C$) of both organic and inorganic carbon in marine and terrestrial records [*Kennett and Stott*, 1991; *Koch et al.*, 1992]. Concurrent with this carbon isotope excursion (CIE), marine sediments show a rapid decrease in calcium carbonate ($CaCO_3$) content [*Colosimo et al.*, 2006; *Thomas and Shackleton*, 1996; *Zachos et al.*, 2005] and a transient global warming of 4–8°C as indicated by various paleothermometers [*Dunkley-Jones et al.*, 2013; *McInerney and Wing*, 2011; *Zachos et al.*, 2003]. This combined evidence points to a massive release of ^{13}C-depleted carbon into the ocean-atmosphere system [*Dickens et al.*, 1997; *Pagani et al.*, 2006]; thus, this interval presents an opportunity to examine the response of ocean chemistry to a geologically rapid increase in the atmospheric concentration of carbon dioxide (CO_2) [*Hönisch et al.*, 2012]. Ocean carbon cycle modeling [*Panchuk et al.*, 2008; *Zeebe et al.*, 2009], using sediment $CaCO_3$ content to constrain the changes in the calcite compensation depth (CCD), estimates the mass of carbon released to between 3000 and 9000 Pg C, with marine methane clathrate, terrestrial and/or marine organic carbon, or some combination thereof as the probable source of carbon [*Dickens et al.*, 1997; *Pagani et al.*, 2006]. In all cases, a significant decrease in surface seawater pH is predicted, the extent of which scales with the rate and magnitude of carbon release [*Hönisch et al.*, 2012; *Ridgwell and Schmidt*, 2010].

Current observational constraints on the changes in the carbonate chemistry of the surface ocean across the Paleocene-Eocene Thermal Maximum (PETM) are largely limited to the abundance and/or morphology of marine calcifiers preserved in sediments [*Bown and Pearson*, 2009; *Gibbs et al.*, 2006, 2010; *Raffi et al.*, 2005], which should be sensitive to rapid ocean acidification. Planktic foraminifers show transient population changes and ecosystem disruption over the PETM, including the temporary disappearance of species abundant before the event, and the evolution of "excursion taxa" [*Kelly et al.*, 1996; *Raffi and De Bernardi*, 2008; *Raffi et al.*, 2009]. In addition, changes in shell morphology may reflect rapid acidification during the CIE followed by elevated saturation during the "overshoot" phase of the recovery [*Kelly et al.*, 1996, 2010]. Calcareous nannoplankton experienced significant yet transient changes in species abundance, though without the major extinction that might be expected during rapid acidification [*Bown and Pearson*, 2009; *Gibbs et al.*, 2006]. Calcareous plankton likely also responded to coeval changes in temperature, salinity, and nutrient concentrations [*Bown and Pearson*,

2009; *Gibbs et al.*, 2010]. Inferring surface ocean saturation from pelagic fossil assemblages is further complicated by preservational biases, such as $CaCO_3$ dissolution at the seafloor [*Gibbs et al.*, 2010]. Therefore, biotic records provide ambiguous evidence of acidification, and we turn to geochemical proxies for independent evidence for ocean acidification.

We used boron-based proxies for reconstructing past variations in seawater carbonate chemistry. In culture experiments, both the boron/calcium ratio (B/Ca) and the boron isotopic composition ($\delta^{11}B$) of planktic foraminifer shells have been shown to reflect carbonate chemistry parameters [*Allen et al.*, 2012; *Henehan et al.*, 2013; *Sanyal et al.*, 1996, 2001]. These relationships are based on the inference from boron isotope studies that the borate ion ($B(OH)_4^-$) is the species predominantly incorporated into calcite [*Hemming and Hanson*, 1992], and both the aqueous abundance of $B(OH)_4^-$ and its isotopic composition increase with seawater pH [*Kakihana et al.*, 1977]. $\delta^{11}B$ in planktic foraminifer shells increases with pH [*Henehan et al.*, 2013; *Hönisch et al.*, 2007; *Sanyal et al.*, 1996, 2001] and has previously been used to reconstruct seawater pH on Pleistocene [*Henehan et al.*, 2013; *Hönisch and Hemming*, 2005] and Cenozoic [*Foster et al.*, 2012; *Pearson et al.*, 2009] timescales. A full understanding of the controls on B/Ca in planktic foraminifera is still emerging, but culturing experiments have demonstrated that B incorporation is well correlated to the ratio of aqueous $B(OH)_4^-$ to total dissolved inorganic carbon (DIC) or bicarbonate (HCO_3^-) [*Allen et al.*, 2011, 2012]. However, quantification of the carbonate chemistry changes documented by B/Ca remains complicated and cannot be used by itself to quantify pH changes [*Allen et al.*, 2012]. In addition, the [B] and $\delta^{11}B$ of ancient seawater are poorly constrained [*Lemarchand et al.*, 2000; *Raitzsch and Hönisch*, 2013; *Simon et al.*, 2006], but the combination of these proxies can be used to reconstruct the timing, duration, and relative magnitude of ocean acidification during the PETM, which can be calculated independently of $\delta^{11}B_{seawater}$ by assuming pre-PETM pH.

2. Materials and Methods

During Ocean Drilling Program (ODP) Leg 198, three holes were drilled at Site 1209 (Shatsky Rise, N. Pacific 32°39.1081′N, 158°30.3564′E) at a water depth of 2387 m [*Bralower et al.*, 2002], equivalent to a paleodepth during the PETM of ~ 1900 m [*Takeda and Kaiho*, 2007]. The Paleocene-Eocene boundary interval, recovered at 109 m composite depth, is composed primarily of a carbonate-rich nannofossil ooze. Investigations of this interval documented a prominent carbon isotope excursion (CIE), warming, carbonate dissolution, and the benthic foraminiferal extinction horizon [*Colosimo et al.*, 2006; *Takeda and Kaiho*, 2007; *Zachos et al.*, 2005]. Site 1209 was chosen for this study because of its location within a subtropical gyre, away from regions of upwelling. Moreover, its high $\%CaCO_3$ and foraminiferal abundance facilitated collection of a high-resolution B/Ca record and large samples for measuring boron isotopes. Sediment samples, collected at 1–3 cm resolution across a 2 m interval spanning the CIE, were washed and sieved, and specimens of the mixed-layer-dwelling planktic species *Morozovella velascoensis* and *Acarinina soldadoensis* were picked from the 250–300 and 300–425 μm size fraction. On the basis of shell size-$\delta^{13}C$ relations, these species likely harbored photosynthetic algal symbionts and were thus restricted to the photic zone of the surface ocean [*D'Hondt et al.*, 1994]. Additionally, specimens of the smooth-walled, thermocline-dwelling genus *Subbotina* were picked from the 250–300 μm size fraction. Isotopic depth ranking suggests that this taxon was nonsymbiotic and occupied the thermocline [*Berggren and Norris*, 1997]. Boron isotope analyses at Site 1209 were restricted to *M. velascoensis* and complemented by low-resolution $\delta^{11}B$ analyses of the same taxon from Sites 1263 (Walvis Ridge, Southeast Atlantic, 28°31.98′S, 02°46.77′E, 2717 m depth; paleodepth ~1500 m; [*Zachos et al.*, 2004]) and 865 (Allison Guyot, Equatorial Pacific, 18°26.41′N, 179°22.24′W, 1518 m depth; paleodepth ~ 1400 m; [*Bralower et al.*, 1995]) to evaluate whether the Site 1209 record is representative of a global signal or compromised by local or preservational effects. At each of these sites, previous work has identified the Paleocene-Eocene (P-E) boundary and accompanying CIE [*Colosimo et al.*, 2006; *Kelly et al.*, 1996; *Zachos et al.*, 2005], which is used to correlate between sites.

We measured $\delta^{11}B$ using standard negative thermal ionization mass spectrometry methods [*Hemming and Hanson*, 1994] and complemented the $\delta^{11}B$ data at Site 1209 by higher-resolution records of B/Ca and Mg/Ca measured by inductively coupled plasma–mass spectrometry, and $\delta^{13}C$ and $\delta^{18}O$ measured by standard dual-inlet techniques (see supporting information for detailed description of analytical methods). In addition to *M. velascoensis*, trace elements and stable isotopes were analyzed in shells of *A. soldadoensis* and *Subbotina*.

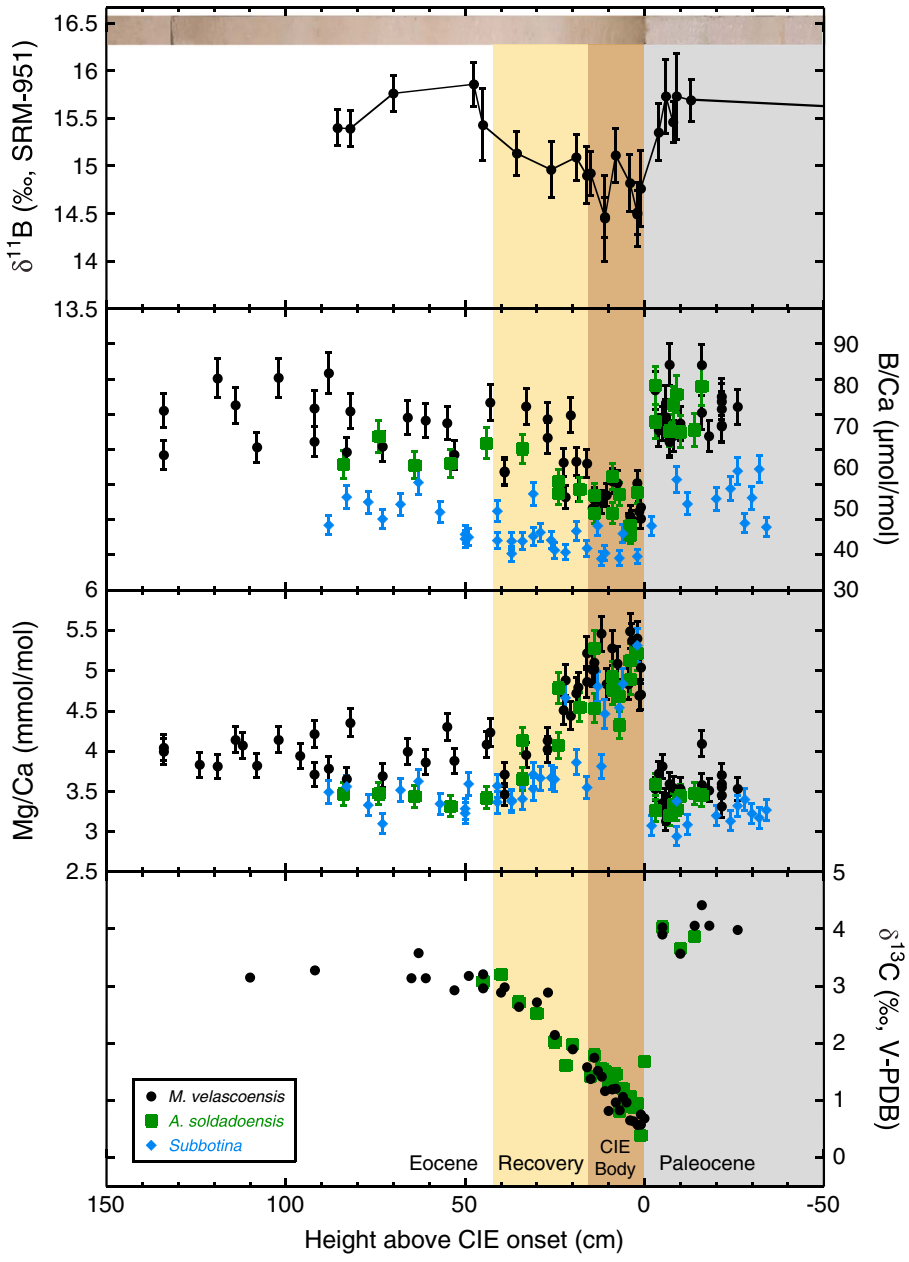

Figure 1. Data from Core 198-1209B-22H plotted against distance in the core in centimeters relative to the CIE onset, at 134 cm in Section 1209B-22H-1W. Shown are a core photograph, foraminiferal $\delta^{11}B$, B/Ca, Mg/Ca, and $\delta^{13}C$ [*Zachos et al.*, 2003]. The grey shaded area indicates the baseline conditions before the onset of the PETM; brown shading indicates the body of the CIE; yellow shading represents the CIE recovery interval; and the unshaded interval is considered postevent. Error bars on Mg/Ca and B/Ca are 2 standard deviations of repeat measurements of an in-house carbonate standard: 7% on B/Ca and 4% on Mg/Ca. Error bars on $\delta^{11}B$ are 2 SE of repeat sample analyses ($n > 3$), or 2 SE of repeat analyses of an in-house vaterite standard given the same n, whichever is larger.

Applying simple assumptions about seawater chemistry (described below and in the supporting information), we estimate not the absolute pH values, but the pH excursion (ΔpH), from $\delta^{11}B$ values across the P-E boundary. As a second constraint, we compare measured B/Ca records with model-derived estimates of B/Ca based on the observed sensitivity of modern foraminifera. These two techniques complement each other in that the more complete understanding of the $\delta^{11}B$ proxy allows a more quantitative interpretation, while the smaller sample size requirement of B/Ca analyses allows generation of a much higher resolution record, so that timing and structure can be resolved more precisely.

Age models were constructed by correlating the fine-fraction $\delta^{13}C$ record of Sites 1209 and 1263 with the bulk $\delta^{13}C$ record for ODP Site 690, which has an orbitally tuned age model [*Röhl et al.*, 2007] (Figure S3). For Site 865, the benthic foraminiferal $\delta^{13}C$ record was correlated with that at Site 690 [*Zachos et al.*, 2001] to generate an age model. Our age models lead to a slightly shorter duration for the CIE than other estimates [*Farley and Eltgroth*, 2003; *Murphy et al.*, 2010]. The resulting age model for Site 1209, similar to that for other pelagic PETM sites, implies greatly reduced sedimentation rates immediately below and within the core of the CIE, resulting from chemical erosion of uppermost Paleocene $CaCO_3$ sediments and decreased production and/or preservation of $CaCO_3$ during the CIE, followed by enhanced sedimentation rates during and after the recovery interval [*Farley and Eltgroth*, 2003], representing a carbonate saturation overshoot phase [*Kelly et al.*, 2010; *Zachos et al.*, 2005].

3. Results

The $\delta^{13}C$ and Mg/Ca values of the mixed-layer-dwelling foraminifera accurately replicate previously published records for Site 1209 [*Zachos et al.*, 2003] and extend them by 200 kyr into the early Eocene (Figure 1). The 50% rise in Mg/Ca (~2 mmol/mol) at the onset of the CIE is consistent with a ~5°C increase in sea surface temperature (SST) [*Zachos et al.*, 2003], whereas the comparably smaller decrease in oxygen isotopes presented in *Zachos et al.* [2003] is consistent with a rise in local $\delta^{18}O_{sw}$ and 1.5 ppt increase in salinity (*S*) [*Zachos et al.*, 2003]. These excursion SST and *S* estimates are used to constrain the boric acid dissociation constant and boron isotopic fractionation factor required for pH calculations from $\delta^{11}B$ across the CIE. Before and after the event, a baseline of 30°C and $S = 37$ are assumed, similar to other estimates of late Paleocene low-latitude SST and *S* [*Kozdon et al.*, 2011].

Site 1209 $\delta^{11}B$ values decrease from an average of ~15.5‰ below the CIE to an average of ~14.7‰ within the body of the CIE (Figure 1). This decrease is rapid, occurring within 5 cm, and values remain low for at least 15 cm (at least 70 kyr) before recovering more gradually to preevent levels, more or less in parallel with the $\delta^{13}C$ recovery. $\delta^{11}B$ values at Sites 1263 and 865 also show a significant decrease within the CIE (Figure 4), supporting that the Site 1209 record reflects global environmental change. However, the excursion is covered by only one or two data points in each of these complementary records, and we therefore restrict calculation of the magnitude of acidification to Site 1209 data.

B/Ca data generally parallel the Site 1209 boron isotope excursion and recovery. The upper Paleocene baseline *M. velascoensis* and *A. soldadoensis* B/Ca values of ~70 μmol/mol fall toward the low end of those of modern symbiont-bearing foraminifers [*Allen et al.*, 2012], consistent with lower than modern seawater pH and [B] [*Lemarchand et al.*, 2000]. Values in both species show a rapid drop from an average of 70 to 45 μmol/mol across the onset of the CIE (Figure 1), remain low for 15 cm (at least ~70 kyr) above the boundary, then recover gradually, in step with $\delta^{11}B$ to pre-CIE levels. B/Ca data for the thermocline-dwelling *Subbotina* follow the same trend as the data for mixed-layer-dwelling species but are offset toward lower values over the entire record, likely reflecting the lower environmental pH of their habitat. *Subbotina* record a smaller B/Ca excursion (from 45 to 30 μmol/mol) than mixed-layer dwellers, consistent with model predictions that the magnitude of acidification decreases with depth in the water column [*Ridgwell and Schmidt*, 2010].

4. Discussion

4.1. Evidence for Acidification

The similarity and timing of the $\delta^{11}B$ and B/Ca anomalies suggest that both proxies are documenting the surface acidification caused by the geologically rapid (within 1 to 20 kyr) release of thousands of Pg C [e.g., *Zeebe and Zachos*, 2012]. However, given the drastic environmental changes documented during the PETM (including warming, salinity changes, and dissolution), we must consider whether there may be factors other than pH that might influence the B proxies.

In culture experiments documenting the sensitivity of planktic foraminiferal $\delta^{11}B$ and B/Ca to pH, no effect was observed with temperature and for B/Ca only a minor effect with salinity (~2.6 μmol/mol/psu) [*Allen et al.*, 2012]. Moreover, culture studies would predict an increase in B/Ca at the PETM onset in response to the local salinity increase [*Zachos et al.*, 2003], the opposite of what is observed. As for preservation artifacts, *Yu et al.* [2007] found no correlation between B/Ca in planktic foraminifers and bottom water carbonate saturation

state (Ω) in core top samples, concluding that seafloor dissolution likely does not alter B/Ca. *Coadic et al.* [2013], however, found a correlation between depth and planktic B/Ca along a depth transect, suggesting that dissolution may be an issue. The observed dissolution effect of 10–15 μmol/mol between 2500 and 5000 m water depth, however, is small compared to the much larger signal in our records, and the paleodepth for Site 1209 was only ~ 1900 m[*Takeda and Kaiho*, 2007]. Similarly, δ^{11}B records have been observed to be affected by dissolution [*Hönisch and Hemming*, 2004], and the change is in the same direction as that observed in our PETM records. Importantly, these dissolution artifacts are associated with a concomitant decrease in Mg/Ca [*Coadic et al.*, 2013; *Hönisch and Hemming*, 2004], whereas our record shows an increase in Mg/Ca, consistent with the global average temperature increase [*Dunkley-Jones et al.*, 2013].

Furthermore, the most extreme phase of dissolution at Site 1209, as reflected in %$CaCO_3$ and shell fragmentation [*Colosimo et al.*, 2006], occurred over ~5 cm during the onset of the event, and dissolution recovered below the δ^{11}B and B/Ca recoveries. Because δ^{11}B and B/Ca remain low after recovery of preservation, we do not consider dissolution a likely explanation for the observed trends. Furthermore, the preservation of species-specific offsets in B/Ca suggests that recrystallization/secondary calcification has not altered the primary signal of the shells. Detailed scanning electron microscope (SEM) photographs of CIE interval planktic foraminifera [*Colosimo et al.*, 2006] provide evidence for some diagenetic carbonate overgrowth and pore infilling, but an overgrowth effect cannot significantly bias our records, given that most of the B in pelagic sediments resides in calcite, pore water contributes comparably little B, and the B/Ca of inorganic calcite is similar to that of biogenic calcite [*Sanyal et al.*, 2000]. A B content similar to that of foraminiferal calcite is most likely in overgrowths, but even if overgrowths contained no B, it would require anomalous carbonate overgrowths of ~30–40% (restricted to only the CIE interval) to explain our B/Ca records, an amount not supported by SEM investigations at Site 1209 [*Colosimo et al.*, 2006]. And, if addition of B-free carbonate overgrowth were to account for the B/Ca decrease, then it could not affect the decrease documented in δ^{11}B. Perhaps the strongest evidence against diagenetic alteration of the δ^{11}B records is the close agreement of resulting pH recorded at three different sites with varied lithologies and diagenetic regimes (see section 4.3).

Additionally, photosynthetic activity of symbiotic algae elevates the pH of the mixed-layer dwellers' calcifying microenvironment [*Hönisch et al.*, 2003; *Jorgensen et al.*, 1985; *Rink et al.*, 1998], but severe warming could have led to the loss of symbionts and thus lowered both δ^{11}B and B/Ca. Symbiont loss has been inferred from a reduced δ^{13}C-shell size relationship during the Middle Eocene Climatic Optimum [*Edgar et al.*, 2013], and culturing studies have documented an effect of symbiont activity on δ^{11}B [*Hönisch et al.*, 2003]. However, the asymbiotic, thermocline-dwelling *Subbotina* also record a B/Ca excursion, which means that potential loss of symbionts cannot explain the entire B/Ca signal.

Additionally, we have measured δ^{11}B in two size fractions (250–300 μm and 300–425 μm) below and during the CIE, as well as within the recovery interval, and there is little or no difference between these size fractions (Table S2). Since symbiont activity affects δ^{11}B-size relationships [*Hönisch and Hemming*, 2004], we conclude that the effects of symbiotic activity or its possible disappearance during the CIE on our δ^{11}B record is minimal. The mixed-layer species might also have migrated to deeper, cooler waters in response to warming, though this seems unlikely because the +5°C temperature increase recorded by Mg/Ca in the same shells is comparable to the global average [*Dunkley-Jones et al.*, 2013; *Sluijs et al.*, 2006; *Zachos et al.*, 2003; *Zachos et al.*, 2006].

We conclude that symbiont loss and/or depth migration cannot explain the entire trends in our records but may have amplified the signal in B/Ca and δ^{11}B in *Morozovella* and *Acarinina*, so that the estimated pH changes should be viewed as maxima if these records are considered complete. However, it is also possible that a short phase of highly acidified conditions at the onset of the CIE is not represented in our B records due to dissolution and chemical erosion. Compared to other pelagic PETM sections, Site 1209 features minimal dissolution, and just a millimeter-scale clay-rich seam [*Colosimo et al.*, 2006] representing the CIE onset. The time represented by this seam is unknown, but local recovery of carbonate deposition from this initial pulse of emissions would be relatively fast ($<$10 kyr), so most of the main portion of CIE is represented as constrained by the correlation between δ^{13}C records (Figure S3).

Finally, changes in the Ca budget related to the global carbonate dissolution pulse [*Komar and Zeebe*, 2011] would produce changes in B/Ca and Mg/Ca much smaller than the analytical uncertainty in the techniques

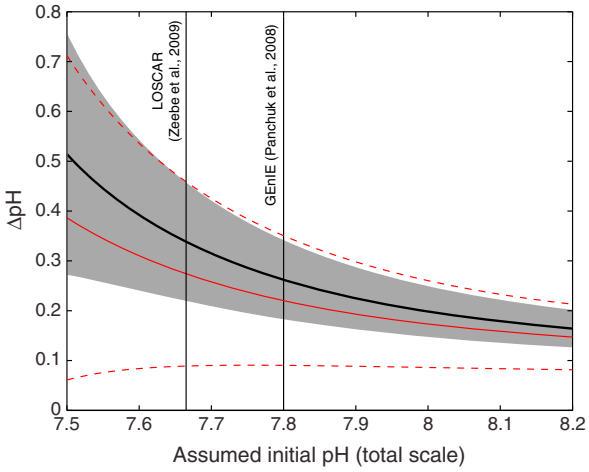

Figure 2. Calculated ΔpH as a function of assumed initial (pre-PETM) pH. Two sets of calculations are shown: (1) (black line and grey shading) δ^{11}B data from the Paleocene ($n = 7$) and the CIE interval ($n = 6$) are treated as populations, and calculations are performed on the variance-weighted mean of those populations with associated uncertainty propagated through the ΔpH calculation (pre-CIE $\delta^{11}B = 15.51‰ \pm 0.12$, CIE $\delta^{11}B = 14.71‰ \pm 0.11$). (2) (red) Only the two δ^{11}B data points spanning the P-E boundary are considered (15.35 ± 0.30 and 14.76 ± 0.40 for the latest Paleocene and earliest Eocene, respectively), and error is analytical uncertainty of δ^{11}B analysis propagated through the ΔpH calculation. Vertical lines represent the preevent pH of two model simulations of the PETM.

employed in this study. Moreover, the B/Ca signals are much larger than the analytical uncertainty, in contrast to those in studies of much smaller pH variations of the late Cenozoic [*Allen and Hönisch*, 2012]. In sum, the potential contributions of complicating factors are minor compared to the magnitude of the anomalies in both the δ^{11}B and B/Ca records. We therefore interpret the decreases in both proxies at the onset of the PETM as ocean acidification signals.

4.2. Quantification of ΔpH From δ^{11}B

To constrain the magnitude of the acidification documented by the B proxies, we calculate a range of ΔpH values from the *M. velascoensis* δ^{11}B record across the CIE onset (pre-PETM values versus CIE values). Computation of absolute pH from foraminiferal δ^{11}B requires knowledge of $\delta^{11}B_{seawater}$, which is unknown for the Paleogene, and of species-specific vital effects, which are difficult to calibrate in these now extinct species. However, $\delta^{11}B_{seawater}$ can be assumed constant over the ~300 kyr time window considered here, because the oceanic residence time of B is >10 Myr [*Lemarchand et al.*, 2000]. Furthermore, estimates of ΔpH independent of those parameters can be made by assuming a pre-PETM baseline pH (see supporting information for full calculations). Using the magnitude of the δ^{11}B-excursion, we calculate ΔpH for a range of assumed initial pH values between 7.5 and 8.2 (Figure 2). Due to reduced sensitivity in the fractionation of B isotopes at lower pH [*Hemming and Hanson*, 1992], the resulting ΔpH is larger at lower assumed initial pH and smaller at high (near-modern) assumed initial pH. Within the range of estimates of pre-PETM pH given by model simulations [*Panchuk et al.*, 2008; *Ridgwell and Schmidt*, 2010; *Zeebe et al.*, 2009], the 0.8‰ decrease in δ^{11}B at the onset of the event is consistent with a ΔpH of −0.27 units, assuming a pre-PETM pH of 7.80 (total scale, consistent with 750 ppm atmospheric CO_2) [*Panchuk et al.*, 2008], to −0.34 units, assuming a pre-PETM pH of 7.67 (total scale, consistent with 1000 ppm CO_2)(Figure 3).

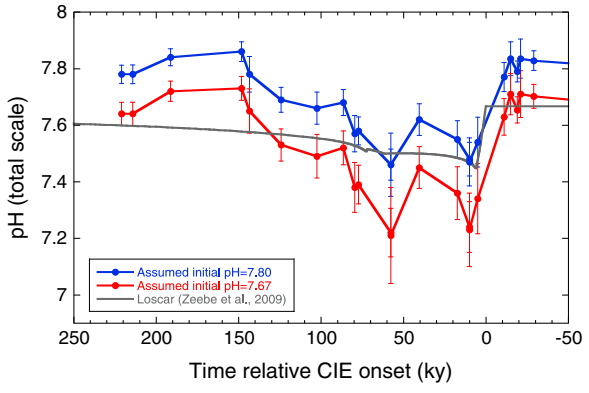

Figure 3. Calculated pH versus time after the onset of the PETM. Two scenarios are plotted, one assuming an initial pH of 7.67 (after *Zeebe et al.* [2009], red) and one assuming initial pH of 7.80 (after *Panchuk et al.* [2008], blue). Error bars reflect 2 SE of individual boron isotope measurements as displayed in Figure 1. For comparison, the grey line shows the evolution of the surface pacific pH in *Zeebe et al.*'s [2009] simulation.

Propagated uncertainties on ΔpH are calculated for two cases (Figure 2): (1) treating the Paleocene and CIE interval δ^{11}B as coherent, normally distributed populations and using a variance-weighted mean with associated propagated uncertainties, and (2) considering only the two δ^{11}B data points which span the P-E boundary and using analytical uncertainty as a source of error (see supporting information for description of statistics and error propagation). Using the weighted mean allows smaller uncertainty (± 0.08 units in the pH = 7.8 pre-PETM case and ± 0.11 units in the pH = 7.67 pre-PETM case)

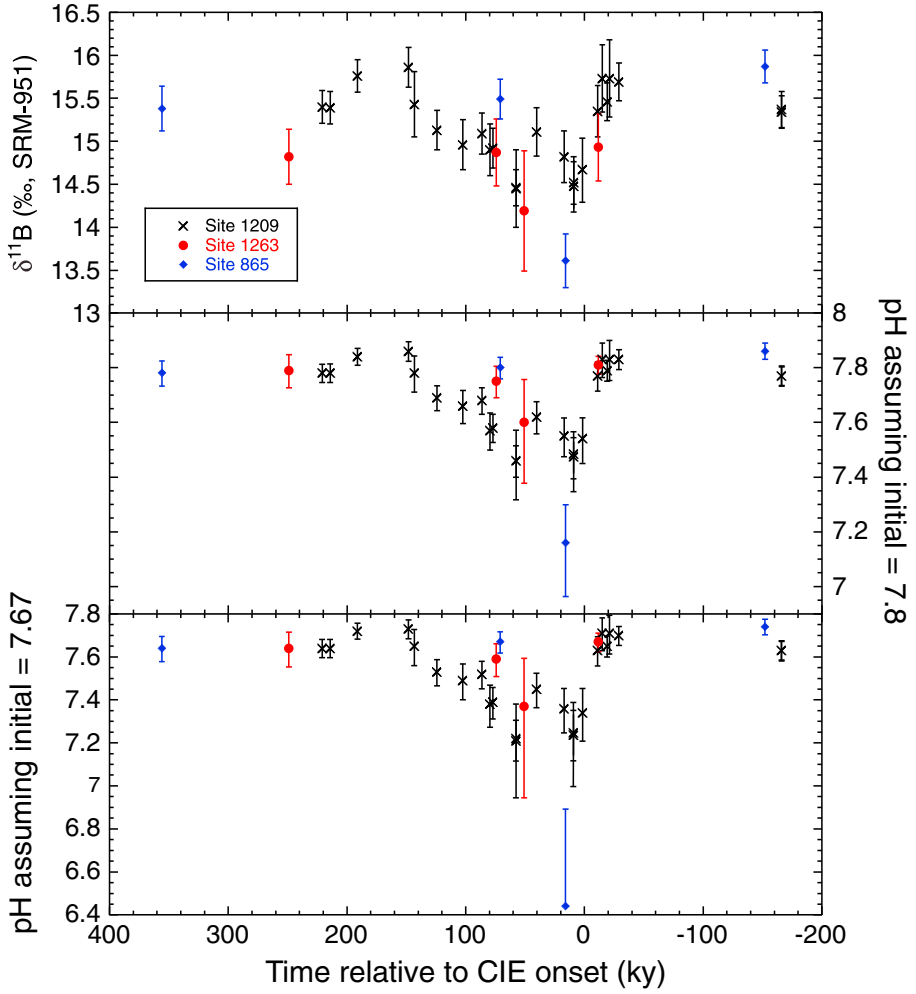

Figure 4. The $\delta^{11}B$ values and two scenarios for pH (total scale) from *M. velascoensis* at all three sites plotted against time. Age models for Sites 1263 and 1209 were produced by correlating the bulk/fine-fraction $\delta^{13}C$ excursion to the $\delta^{13}C$ excursion at Site 690 in the age model of [*Röhl et al.*, 2007]; for Site 865 the benthic foraminiferal $\delta^{13}C$ record [*Zachos et al.*, 2001] was correlated to that at Site 690, using the same age model. Error bars on $\delta^{11}B$ are 2 SE of repeat analyses ($n > 3$) or 2 SE of repeat analyses of an in-house vaterite standard given the same n, whichever is larger. The pH in the middle and lower panels were calculated by assuming the initial pH for the Site 1209 record of 7.8 and 7.67 (total scale), respectively, and then applying the same $\delta^{11}B$-pH relationship to all sites. Error bars reflect the uncertainty reported for $\delta^{11}B$ analyses. The lower error bar on one point in the CIE from Site 865 is incalculable because the lower error limit on the $\delta^{11}B$ of that point is below the minimum $\delta^{11}B$ in the $\delta^{11}B$-pH relationship.

than the second technique (± 0.13 units in the pH = 7.8 pre-PETM case and ± 0.18 units in the pH = 7.67 pre-PETM case). The first technique, however, rests on the assumption that the two populations of $\delta^{11}B$ are normally distributed around a coherent mean, which may not be the case, especially within the CIE when pH likely varied over time (Figure 5c). The second technique avoids this assumption, but the two boundary-spanning data points are separated by 16 kyr in our age model, so that this comparison does not necessarily capture the full magnitude of the ΔpH across the boundary.

Applying the same vital effect offset and $\delta^{11}B_{seawater}$ values at Sites 1209, 865, and 1263, pre-PETM pH estimates from $\delta^{11}B$ are within ±0.05 pH units (Figure 4), suggesting that diagenesis is not a major concern, because it would have affected the three sites differently due to different burial depths, carbonate content, bottom water, and pore water chemistry. The P-E interval at Site 865 (paleodepth ~1400 m) is a winnowed foraminiferal sand (nearly 100% $CaCO_3$), bearing planktic foraminifers with significant overgrowth [*Kelly et al.*, 1996; *Kozdon et al.*, 2013]. Site 1209 (paleodepth ~1900 m) foraminifers are lightly overgrown [*Colosimo et al.*, 2006], while Site 1263 (paleodepth ~1500 m) features clay-rich sediments (~85% $CaCO_3$)

with excellent foraminiferal preservation [*Kelly et al.*, 2010] but a larger clay layer indicating more intense dissolution [*Zachos et al.*, 2005]. Depending on the initial pH, our Site 1209 $\delta^{11}B$ data allow for a wide range of ΔpH values (i.e., larger if a lower initial pH is assumed and smaller if a higher initial pH is assumed; Figure 2), though an initial pH far outside the range in Figure 2, and assuming realistic values for other carbonate chemistry parameters, would be irreconcilable with independent estimates for Paleocene pCO_2 [*Beerling and Royer*, 2011].

4.3. Significance of the B/Ca Excursion

The B/Ca data allow us to independently evaluate the magnitude of acidification in surface waters at the onset of the PETM. Based on theoretical and laboratory studies, a pH decrease as estimated from the anomaly in $\delta^{11}B$ should also lower the B/Ca of foraminifera [*Allen et al.*, 2012], as indeed recorded at Site 1209. In order to estimate changes in pH from B/Ca, however, we must apply calibrations for modern foraminifer species, which, in contrast to $\delta^{11}B$ versus pH relationships, vary in sensitivity between species. We assume that extinct species shared a similar range of sensitivities as living species, but the approach is complicated by the dual response of planktic B/Ca to varying $[B(OH)_4^-]$ and DIC, where carbonate and borate ion appear to compete for lattice sites during calcification[*Allen et al.*, 2012]. Although the concentrations of aqueous borate and carbonate ions are coupled during a rapid ocean acidification event and fall with decreasing pH [*Zeebe et al.*, 2009], the carbon pulse at the onset of the PETM led to an increase in DIC, which may have amplified the B/Ca decrease through decreasing $[B(OH)_4^-]$/DIC (Figure 5c). In the later phase of the event (>10 kyr after the CIE onset), terrestrial weathering increased the flux of alkalinity and DIC to the ocean which decoupled pH and carbonate ion concentration [*Hönisch et al.*, 2012], leading to slower recovery of $[B(OH)_4^-]$/DIC (and thus B/Ca) than surface ocean carbonate saturation (Figure 5c). As such, a direct, quantitative estimate of carbonate chemistry from raw B/Ca data carries uncertainty at present. Nevertheless, the direction, magnitude, and timing of the B/Ca excursions are qualitatively consistent with rapid and sustained reductions in thermocline and surface ocean pH, lasting as long as the peak carbon isotope excursion (>70 kyr).

4.4. Model-Data Comparison

Within the limitations of these uncertainties, we employed a simple strategy to evaluate the magnitude of ocean acidification in our B/Ca record through comparison with modeled environmental parameters. *Zeebe et al.* [2009] simulated PETM carbon release with a global carbon cycle model Long-term Ocean-atmosphere-Sediment CArbon cycle Reservoir model (LOSCAR) constrained by observations of the global CIE and sediment $\%CaCO_3$ which document changes in the position of the CCD. The best fit to available data involves the rapid release of 3000 Pg C in 6 kyr, followed by an additional release of 1480 Pg C over the following 72 kyr. This results in an ~700 ppmv CO_2 increase, ~0.18 unit surface pH decrease (Figure 3), and 25% reduction in surface carbonate saturation state. To estimate how modern foraminiferal B/Ca would respond to this scenario, we applied empirical calibrations [*Allen et al.*, 2011, 2012] that relate B/Ca in the modern species *Globigerinoides ruber*, *Globigerinoides sacculifer*, and *Orbulina universa* to ($[B(OH)_4^-]$/DIC). Two interpretations of the culture-based calibrations are used: (a) B/Ca responds to absolute changes in $[B(OH)_4^-]$/DIC, and (b) B/Ca responds to the relative change in $[B(OH)_4^-]$/DIC. The latter may be more appropriate for the PETM because the initial (preevent) $[B(OH)_4^-]$/DIC predicted by the model is very different from the value in modern seawater in culture experiments (see supporting information and Figure S1). In both cases, $[B(OH)_4^-]$/DIC is largely controlled by pH, with additional amplification due to increasing DIC from the carbon input, carbonate dissolution, and enhanced weathering. We then compared these model-derived B/Ca estimates with the measured B/Ca of the PETM mixed-layer dwellers (Figure 5).

Predicting baseline B/Ca using model-derived pH and DIC constraints combined with modern proxy calibrations yields B/Ca values within the range of observed pre-PETM B/Ca values (Figure 5), implying that the extinct species incorporated boron in roughly the same proportion as some modern species. The model-derived curves also match the overall shape of the B/Ca excursion: a rapid decrease at the CIE onset, followed by an interval of low values that roughly coincides with the duration of the global CIE, and finally a gradual recovery. However, our model-derived B/Ca curves predict a decrease of only 6–8% for the absolute calibrations, 10–25% for the relative calibrations at the onset of the PETM (Figure 5b), as compared to the much larger ~40% decline recorded by fossil shells across the PETM. This suggests that, at face value, the B/Ca data indicate more severe acidification than predicted by the model. Similarly, the LOSCAR best fit

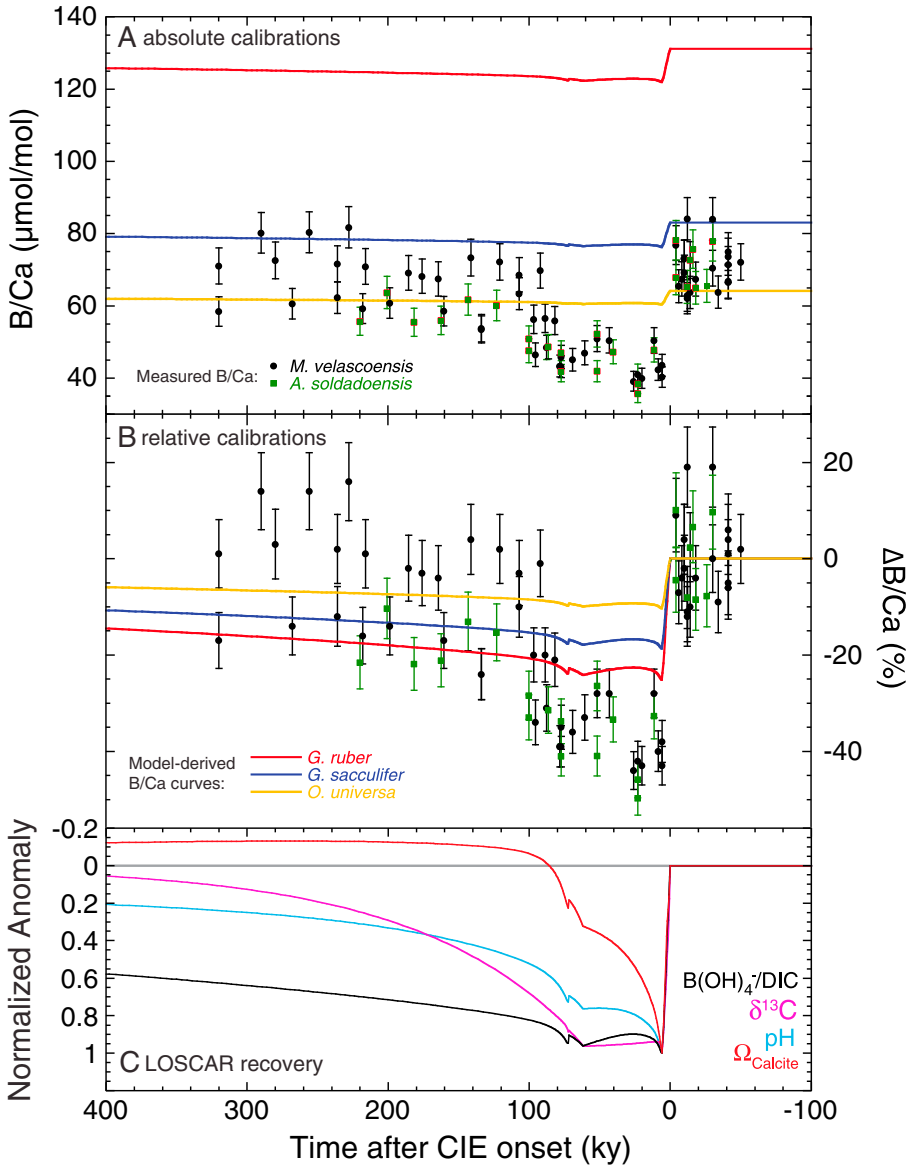

Figure 5. Model-data comparison of the PETM B/Ca anomaly. Symbols with error bars are B/Ca measured in mixed-layer-dwelling foraminifers from Core 198-1209B-22H, plotted against a timescale derived from correlating the fine-fraction CIE at that site to the orbitally tuned age model of ODP Site 690 [*Röhl et al.*, 2007] (see supporting information Figure S3). Note that this age model produces a conservative estimate of the CIE duration (~100 kyr) compared to other age models which suggest a duration up to ~200 kyr [*Murphy et al.*, 2010], so time after the CIE onset of the B/Ca data should be taken as a minimum. Colored lines are model-derived predictions generated by applying the "absolute" and "relative" cultured B/Ca calibrations of three modern foraminifer species [*Allen et al.*, 2011, 2012] to the mixed-layer water carbonate chemistry conditions calculated for the low-latitude surface Pacific by the best fit PETM simulation of the LOSCAR carbon cycle model [*Zeebe et al.*, 2009] (see supporting information for discussion of timescale and calibrations). (a) Measured B/Ca ratios (μmol/mol) compared with model-derived curves using the absolute calibration. (b) The B/Ca anomaly as percent change relative to the Paleocene baseline along with model-derived curves using the relative calibration. (c) Normalized excursions in pH, surface Pacific $\delta^{13}C$, $\Omega_{calcite}$, and $B(OH)_4^-/DIC$ (where 0 represents initial Paleocene values and 1 represents PETM minima) demonstrating the different timescales of recovery between model parameters. Horizontal grey line represents preevent conditions for all parameters.

simulation [*Zeebe et al.*, 2009] involves a total ~4500 Pg C input and results in an ~0.18 pH unit decrease, whereas the $\delta^{11}B$ data imply a ΔpH of -0.33 units if calibrated to LOSCAR's initial pH of 7.67 (total scale), also a significantly greater acidification than simulated by the model. There are several potential explanations for the greater acidification implied by both B/Ca and $\delta^{11}B$ than predicted by the model.

In addition to the possible minor amplification of symbiont loss discussed above, the partitioning of B/Ca in extinct species might have been more sensitive to changes in carbonate chemistry than in modern species. This is unlikely, given that their B/Ca values are at the low end of the range reported from modern foraminifera, thus consistent with what modern foraminifera living in low pH [*Hönisch et al.*, 2012] and low [B] [*Lemarchand et al.*, 2000] Paleogene seawater might record.

Differences in [B] and $[B(OH)_4^-]$/DIC of Paleogene seawater chemistry from culture calibration conditions [*Allen et al.*, 2012] or the initial boundary conditions of model simulations represent a source of uncertainty. For example, models for the late Paleocene estimate a total [B] of seawater 10% lower than modern [*Lemarchand et al.*, 2000], and [Ca] may have been twice as high as modern [*Tyrrell and Zeebe*, 2004]. Also, the LOSCAR simulations are run from an equilibrium concentration of 1000 ppmv atmospheric CO_2, but Paleocene CO_2 levels may have differed by several hundred ppmv (e.g., *Panchuk et al*. [2008] use an initial pCO_2 of 750 ppmv), which would affect the initial $[B(OH)_4^-]$/DIC ratio in the model, as well as require a smaller ΔpH based on $\delta^{11}B$ (Figure 2).

A final potential explanation is that the one standard simulation considered in this paper underestimates the mass of carbon released during the PETM or does not capture the sensitivity of simulated pH changes to variations in model parameters. The large ΔpH estimated from our Site 1209 $\delta^{11}B$ and B/Ca appears more consistent with the upper end of the range of estimates of modeling studies constrained by other observational constraints on ocean carbonate chemistry (i.e., the CCD) [*Panchuk et al.*, 2008; *Ridgwell and Schmidt*, 2010; *Zeebe et al.*, 2009]. Such comparisons with models, however, hinge on a number of key assumptions, including the initial boundary conditions for ocean chemistry including DIC, pH, initial depth of the CCD, and more. For instance, the simulated ΔpH in the standard run is ~0.18 units at $t = 20$ kyr after the onset. However, in a simulation including a moderate rise in remineralization of marine organic carbon at intermediate depth in response to the PETM warming [*Matsumoto*, 2007; *Zeebe*, 2013] and small changes in the timing of the gradual, additional carbon release, ΔpH is ~0.24 units at $t = 20$ kyr. This number is closer to the ~0.3 units based on $\delta^{11}B$ and illustrates the sensitivity of model-calculated ΔpH to parameters other than carbon input. Similarly, simply initializing LOSCAR to a higher initial surface pH (lower atmospheric pCO_2 concentration) would help reconcile the modeled ΔpH with that based on $\delta^{11}B$ without invoking larger carbon release. Importantly, invoking a larger carbon release during the PETM would have to be reconciled with other observations, specifically the response of the CCD. Records of weight $\%CaCO_3$ at Pacific drill sites constrain the initial CCD shoaling in that basin to less than 500 m at the onset of the PETM, and modeling simulations invoking a larger carbon release (without compensatory effects such as changing ocean circulation) result in much more pronounced shoaling of the Pacific CCD than observed [*Sluijs et al.*, 2012].

There are implications for two aspects of the duration and rate of recovery of acidification in our records compared to model simulations. First, the duration of acidified conditions as indicated by the $\delta^{11}B$ and B/Ca record is long, at least 70 kyr. Both GENIE [*Panchuk et al.*, 2008] and LOSCAR [*Zeebe et al.*, 2009] simulations of the PETM are unable to sustain acidified surface ocean conditions for this duration with a single brief ($<$10 kyr) pulse of carbon at the onset of the event. A sustained acidification is more consistent with a scenario of a large, rapid initial pulse of carbon, followed by a slower, gradual release of carbon, perhaps as a feedback to the initial release [*Zeebe*, 2013; *Zeebe et al.*, 2009]. Such a gradual release must have persisted as long as the CIE, or a minimum of ~70 kyr using our age model (Figure S3). Alternatively, the sustained acidification could result from multiple emission pulses of carbon spaced sufficiently close together (tens of kyr apart) that pH does not have time to recover between pules, though there is no obvious evidence for such in marine or continental carbon isotope records. Second, the recovery in $\delta^{11}B$ and B/Ca values is faster ($<$200 kyr) than the $>$400 kyr duration in the LOSCAR simulation, and this is not an artifact of age models. For example, had we used the age model of *Murphy et al.* [2010], the recovery in our proxies would be more gradual (occurring over ~150 kyr rather than the ~100 kyr in our age model) but not nearly as prolonged as in the model. This may indicate that B/Ca could actually track a carbonate chemistry parameter other than $[B(OH)_4^-]$/DIC or a combination of parameters including Ω, which would be consistent with Ω recovering more quickly than other parameters in our simulation (Figure 5). Alternatively, the recovery may have been accelerated by carbon removal processes not accounted for in the model, such as enhanced organic burial [*Bowen and Zachos*, 2010]. As the simulation of surface saturation is highly sensitive to model-dependent feedbacks (i.e., weathering, export production, etc.), some of which can vary regionally, a full assessment requires data from multiple locations and further analysis.

5. Conclusions

Our records indicate abrupt and sustained acidification of the upper ocean coincident with the onset of the PETM, consistent with a scenario of massive carbon release. The magnitude of acidification (ΔpH of about 0.3 units) appears most consistent with the upper end of carbon release scenarios, although this calculation is subject to significant uncertainties. The timing of the $\delta^{11}B$ and B/Ca excursions is tightly coupled to the Mg/Ca-based temperature excursion (Figure S2), confirming the link between low pH/high pCO_2 and globally elevated temperatures. The total cumulative mass of carbon released during the PETM may have been similar to that anticipated for future anthropogenic carbon emissions of 5000 Pg C, but the rate of carbon release was likely at least an order of magnitude slower [*Zeebe and Zachos*, 2012] resulting in significantly more gradual and less severe surface ocean acidification. Calcareous plankton may thus have had the opportunity to adapt, either through migration or possibly through evolution [*Hönisch et al.*, 2012]. Therefore, the lack of major extinction of planktic calcifiers during the PETM cannot be taken as evidence that modern calcifiers are insensitive to anthropogenic ocean acidification.

Acknowledgments
We thank Dyke Andreasen, Linda Anderson, Rob Franks, and Jeremy Hourigan for technical support and Steve Bohaty for supplying Site 1209 fine-fraction stable isotope data. Andy Ridgwell, Tim Bralower, Tim Lyons, and five anonymous reviewers provided productive feedback on different versions of the manuscript. This work was funded by the US National Science Foundation under grants OCE-0903014, OCE09-02869, OCE12-20602, and OCE12-20554.

References

Allen, K. A., and B. Hönisch (2012), The planktic foraminiferal B/Ca proxy for seawater carbonate chemistry: A critical evaluation, *Earth Planet. Sci. Lett.*, *345–348*, 203–211.
Allen, K. A., B. Hönisch, S. M. Eggins, J. Yu, H. J. Spero, and H. Elderfield (2011), Controls on boron incorporation in cultured tests of the planktic foraminifer *Orbulina universa*, *Earth Planet. Sci. Lett.*, *309*(3), 291–301.
Allen, K. A., B. Hönisch, S. M. Eggins, and Y. Rosenthal (2012), Environmental controls on B/Ca in calcite tests of the tropical planktic foraminifer species *Globigerinoides ruber* and *Globigerinoides sacculifer*, *Earth Planet. Sci. Lett.*, *351–352*, 270–280.
Beerling, D., and D. L. Royer (2011), Convergent Cenozoic CO_2 history, *Nat. Geosci.*, *4*, 418–420.
Berggren, W. A., and R. D. Norris (1997), Biostratigraphy, phylogeny and systematics of Paleocene trochospiral planktic foraminifera, *Micropaleontol*, *43*, 1–116.
Bowen, G. J., and J. C. Zachos (2010), Rapid carbon sequestration at the termination of the Palaeocene-Eocene Thermal Maximum, *Nat. Geosci.*, *3*(12), 866–869.
Bown, P., and P. Pearson (2009), Calcareous plankton evolution and the Paleocene/Eocene Thermal Maximum event: New evidence from Tanzania, *Mar. Micropaleontol.*, *71*(1–2), 60–70.
Bralower, T. J., J. C. Zachos, E. Thomas, M. Parrow, C. K. Paull, D. C. Kelly, I. P. Silva, W. V. Sliter, and K. C. Lohmann (1995), Late Paleocene to Eocene paleoceanography of the equatorial Pacific Ocean—Stable isotopes recorded at Ocean Drilling Program Site 865, Allison Guyot, *Paleceanography*, *10*(4), 841–865.
Bralower, T. J., et al. (2002), *Proceedings of the Ocean Drilling Program, Initial Reports*, Ocean Drilling Program, College Station, Tex.
Coadic, R., F. Bassinot, D. Dissard, E. Douville, M. Greaves, and E. Michel (2013), A core-top study of dissolution effect on B/Ca in *Globigerinoides sacculifer* from the tropical Atlantic: Potential bias for paleo-reconstruction of seawater carbonate chemistry, *Geochem. Geophys. Geosyst.*, *14*, 1053–1068, doi:10.1029/2012GC004296.
Colosimo, A. B., T. J. Bralower, and J. C. Zachos (2006), Evidence for lysocline shoaling and methane hydrate dissociation at the Paleocene-Eocene Thermal Maximum on Shatsky Rise, ODP Leg 198, in *Proceedings of the Ocean Drilling Program—Scientific Results*, edited by T. J. Bralower, I. Premoli Silva, and M. Malone, pp. 1–36, Ocean Drilling Program, College Station, Tex.
D'Hondt, S., J. C. Zachos, and G. Schultz (1994), Stable isotopic signals and photosymbiosis in Late Paleocene planktic foraminifera, *Paleobiology*, *20*(3), 391–406.
Dickens, G. R., M. M. Castillo, and J. C. G. Walker (1997), A blast of gas in the latest Paleocene: Simulating first-order effects of massive dissociation of oceanic methane hydrate, *Geology*, *25*(3), 259–262.
Dunkley-Jones, T., D. J. Lunt, D. N. Schmidt, A. Ridgwell, A. Sluijs, P. J. Valdes, and M. Maslin (2013), Climate model and proxy data constraints on ocean warming across the Paleocene-Eocene Thermal Maximum, *Earth Sci. Rev.*, *125*, 123–145.
Edgar, K., S. Bohaty, S. Gibbs, P. Sexton, R. Norris, and P. Wilson (2013), Symbiont 'bleaching' in planktic foraminifera during the Middle Eocene Climatic Optimum, *Geology*, *41*(1), 15–18.
Farley, K. A., and S. F. Eltgroth (2003), An alternative age model for the Paleocene-Eocene Thermal Maximum using extraterrestrial He-3, *Earth Planet. Sci. Lett.*, *208*(3–4), 135–148.
Foster, G. L., C. H. Lear, and J. W. Rae (2012), The evolution of pCO_2, ice volume and climate during the middle Miocene, *Earth Planet. Sci. Lett.*, *341*, 243–254.
Gibbs, S. J., P. R. Bown, J. A. Sessa, T. J. Bralower, and P. A. Wilson (2006), Nannoplankton extinction and origination across the Paleocene-Eocene Thermal Maximum, *Science*, *314*(5806), 1770–1773.
Gibbs, S. J., H. M. Stoll, P. R. Bown, and T. J. Bralower (2010), Ocean acidification and surface water carbonate production across the Paleocene-Eocene Thermal Maximum, *Earth Planet. Sci. Lett.*, *295*(3–4), 583–592.
Hemming, N. G., and G. N. Hanson (1992), Boron isotopic composition and concentration in modern marine carbonates, *Geochim. Cosmochim. Acta*, *56*, 537–543.
Hemming, N. G., and G. N. Hanson (1994), A procedure for the isotopic analysis of boron by negative thermal ionization mass spectrometry, *Chem. Geol.*, *114*, 147–156.
Henehan, M. J., et al. (2013), Calibration of the boron isotope proxy in the planktonic foraminifera *Globigerinoides ruber* for use in palaeo-CO_2 reconstruction, *Earth Planet. Sci. Lett.*, *364*, 111–122.
Hönisch, B., and N. G. Hemming (2004), Ground-truthing the boron isotope paleo-pH proxy in planktonic foraminifera shells: Partial dissolution and shell size effects, *Paleoceanography*, *19*, PA4010, doi:10.1029/2004PA001026.
Hönisch, B., and N. G. Hemming (2005), Surface ocean pH response to variations in pCO_2 through two full glacial cycles, *Earth Planet. Sci. Lett.*, *236*(1–2), 305–314.

Hönisch, B., J. Bijma, A. D. Russell, H. J. Spero, M. R. Palmer, R. E. Zeebe, and A. Eisenhauer (2003), The influence of symbiont photosynthesis on the boron isotopic composition of foraminifera shells, *Mar. Micropaleontol.*, *49*(1–2), 87–96.
Hönisch, B., N. G. Hemming, and B. Loose (2007), Comment on "A critical evaluation of the boron isotope-pH proxy: The accuracy of ancient ocean pH estimates" by M. Pagani, D. Lemarchand, A. Spivack and J. Gaillardet, *Geochim. Cosmochim. Acta*, *71*(6), 1636–1641.
Hönisch, B., et al. (2012), The geological record of ocean acidification, *Science*, *335*(6072), 1058–1063.
Jorgensen, B. B., J. Erez, N. P. Revsbech, and Y. Cohen (1985), Symbiotic photosynthesis in a planktonic foraminiferan, *Globigerinoides sacculifer* (Brady), studied with microelectrodes, *Limnol. Oceanogr.*, *30*(6), 1253–1267.
Kakihana, H., M. Kotaka, S. Satoh, M. Nomura, and M. Okamoto (1977), Fundamental studies on the ion-exchange of boron isotopes, *Bull. Chem. Soc. Japn.*, *50*, 158–163.
Kelly, D. C., T. J. Bralower, J. C. Zachos, I. P. Silva, and E. Thomas (1996), Rapid diversification of planktonic foraminifera in the tropical Pacific (ODP Site 865) during the Late Paleocene Thermal Maximum, *Geology*, *24*(5), 423–426.
Kelly, D. C., T. M. J. Nielsen, H. K. McCarren, J. C. Zachos, and U. Rohl (2010), Spatiotemporal patterns of carbonate sedimentation in the South Atlantic: Implications for carbon cycling during the Paleocene-Eocene Thermal Maximum, *Palaeogeogr. Palaeoclimatol. Palaeoecol.*, *293*(1–2), 30–40.
Kennett, J. P., and L. D. Stott (1991), Abrupt deep-sea warming, palaeoceanographic changes and benthic extinctions at the end of the Palaeocene, *Nature*, *353*(6341), 225–229.
Koch, P. L., J. C. Zachos, and P. D. Gingerich (1992), Correlation between isotope records in marine and continental carbon reservoirs near the Palaeocene Eocene boundary, *Nature*, *358*(6384), 319–322.
Komar, N., and R. Zeebe (2011), Oceanic calcium changes from enhanced weathering during the Paleocene-Eocene Thermal Maximum: No effect on calcium-based proxies, *Paleoceanography*, *26*, PA3211, doi:10.1029/2010PA001979.
Kozdon, R., D. C. Kelly, N. T. Kita, J. H. Fournelle, and J. W. Valley (2011), Planktonic foraminiferal oxygen isotope analysis by ion microprobe technique suggests warm tropical sea surface temperatures during the Early Paleogene, *Paleoceanography*, *26*, PA3206, doi:10.1029/2010PA002056.
Kozdon, R., D. Kelly, K. Kitajima, A. Strickland, J. Fournelle, and J. Valley (2013), In situ δ18O and Mg/Ca analyses of diagenetic and planktic foraminiferal calcite preserved in a deep-sea record of the Paleocene-Eocene Thermal Maximum, *Paleoceanography*, *28*, 517–528, doi:10.1002/palo.20048.
Lemarchand, D., J. Gaillardet, É. Lewin, and C. J. Allègre (2000), The influence of rivers on marine boron isotopes and implications for reconstructing past ocean pH, *Nature*, *408*, 951–954.
Matsumoto, K. (2007), Biology-mediated temperature control on atmospheric pCO_2 and ocean biogeochemistry, *Geophys. Res. Lett.*, *34*, L20605, doi:10.1029/2007GL031301.
McInerney, F. A., and S. Wing (2011), The Paleocene-Eocene Thermal Maximum: A perturbation of carbon cycle, climate, and biosphere with implications for the future, *Annu. Rev. Earth Planet. Sci.*, *39*, 489–516.
Murphy, B. H., K. A. Farley, and J. C. Zachos (2010), An extraterrestrial He-3-based timescale for the Paleocene-Eocene Thermal Maximum (PETM) from Walvis Ridge, IODP Site 1266, *Geochim. Cosmochim. Acta*, *74*(17), 5098–5108.
Pagani, M., K. Caldeira, D. Archer, and J. C. Zachos (2006), An ancient carbon mystery, *Science*, *314*(5805), 1556–1557.
Panchuk, K., A. Ridgwell, and L. R. Kump (2008), Sedimentary response to Paleocene-Eocene Thermal Maximum carbon release: A model-data comparison, *Geology*, *36*(4), 315–318.
Pearson, P. N., G. L. Foster, and B. S. Wade (2009), Atmospheric carbon dioxide through the Eocene-Oligocene climate transition, *Nature*, *461*(7267), 1110–1113.
Raffi, I., and B. De Bernardi (2008), Response of calcareous nannofossils to the Paleocene–Eocene Thermal Maximum: Observations on composition, preservation and calcification in sediments from ODP Site 1263 (Walvis Ridge—SW Atlantic), *Mar. Micropaleontol.*, *69*(2), 119–138.
Raffi, I., J. Backman, and H. Palike (2005), Changes in calcareous nannofossil assemblages across the Paleocene/Eocene transition from the paleo-equatorial Pacific Ocean, *Palaeogeogr. Palaeoclimatol. Palaeoecol.*, *226*(1–2), 93–126.
Raffi, I., J. Backman, J. C. Zachos, and A. Sluijs (2009), The response of calcareous nannofossil assemblages to the Paleocene Eocene Thermal Maximum at the Walvis Ridge in the South Atlantic, *Mar. Micropaleontol.*, *70*(3–4), 201–212.
Raitzsch, M., and B. Hönisch (2013), Cenozoic boron isotope variations in benthic foraminifers, *Geology*, *41*(5), 591–594.
Ridgwell, A., and D. N. Schmidt (2010), Past constraints on the vulnerability of marine calcifiers to massive carbon dioxide release, *Nat. Geosci.*, *3*, 196–200.
Rink, S., M. Kühl, J. Bijma, and H. J. Spero (1998), Microsensor studies of photosynthesis and respiration in the symbiotic foraminifer *Orbulina universa*, *Mar. Biol.*, *131*(4), 583–595.
Röhl, U., T. Westerhold, T. J. Bralower, and J. C. Zachos (2007), On the duration of the Paleocene-Eocene Thermal Maximum (PETM), *Geochem. Geophys. Geosyst.*, *8*, Q12002, doi:10.1029/2007GC001784.
Sanyal, A., N. G. Hemming, W. S. Broecker, D. W. Lea, H. J. Spero, and G. N. Hanson (1996), Oceanic pH control on the boron isotopic composition of foraminifera—Evidence from culture experiments, *Paleoceanography*, *11*(5), 513–517, doi:10.1029/96PA01858.
Sanyal, A., M. Nugent, R. J. Reeder, and J. Bijma (2000), Seawater pH control on the boron isotopic composition of calcite: Evidence from inorganic calcite precipitation experiments, *Geochim. Cosmochim. Acta*, *64*(9), 1551–1555.
Sanyal, A., J. Bijma, H. J. Spero, and D. W. Lea (2001), Empirical relationship between pH and the boron isotopic composition of *Globigerinoides sacculifer*: Implications for the boron isotope paleo-pH proxy, *Paleoceanography*, *16*(5), 515–519, doi:10.1029/2000PA000547.
Simon, L., C. Lecuyer, C. Marechal, and N. Coltice (2006), Modelling the geochemical cycle of boron: Implications for the long-term $\delta^{11}B$ evolution of seawater and oceanic crust, *Chem. Geol.*, *22*(1–2), 15.
Sluijs, A., et al. (2006), Subtropical arctic ocean temperatures during the Palaeocene/Eocene Thermal Maximum, *Nature*, *441*(7093), 610–613.
Sluijs, A., J. C. Zachos, and R. E. Zeebe (2012), Constraints on hyperthermals, *Nat. Geosci.*, *5*(4), 231–231.
Takeda, K., and K. Kaiho (2007), Faunal turnovers in central Pacific benthic foraminifera during the Paleocene–Eocene Thermal Maximum, *Palaeogeogr. Palaeoclimatol. Palaeoecol.*, *251*(2), 175–197.
Thomas, E., and N. J. Shackleton (1996), The Paleocene-Eocene benthic foraminiferal extinction and stable isotope anomalies, in *Correlation of the Early Paleogene in Northwest Europe*, Special Publications, vol. 101, edited by R. W. O. B. Knox, R. M. Corfield, and R. E. Dunay, pp. 401–441, Geol. Soc., London.
Tyrrell, T., and R. E. Zeebe (2004), History of carbonate ion concentration over the last 100 million years, *Geochim. Cosmochim. Acta*, *68*(17), 3521–3530.
Yu, J., H. Elderfield, and B. Hönisch (2007), B/Ca in planktonic foraminifera as a proxy for surface seawater pH, *Paleoceanography*, *22*, PA2202, doi:10.1029/2006PA001347.

Zachos, J., M. Pagani, L. Sloan, E. Thomas, and K. Billups (2001), Trends, rhythms, and aberrations in global climate 65 Ma to present, *Science*, *292*(5517), 686–693.

Zachos, J. C., M. W. Wara, S. Bohaty, M. L. Delaney, M. R. Petrizzo, A. Brill, T. J. Bralower, and I. Premoli-Silva (2003), A transient rise in tropical sea surface temperature during the Paleocene-Eocene Thermal Maximum, *Science*, *302*(5650), 1551–1554.

Zachos, J. C., et al. (2004), *Proceedings of the Ocean Drilling Program, Initial Reports*, Ocean Drilling Program, College Station, Tex.

Zachos, J. C., et al. (2005), Rapid acidification of the ocean during the Paleocene-Eocene Thermal Maximum, *Science*, *308*(5728), 1611–1615.

Zachos, J. C., S. Schouten, S. Bohaty, T. Quattlebaum, A. Sluijs, H. Brinkhuis, S. J. Gibbs, and T. J. Bralower (2006), Extreme warming of mid-latitude coastal ocean during the Paleocene-Eocene Thermal Maximum: Inferences from TEX86 and isotope data, *Geology*, *34*(9), 737–740.

Zeebe, R. E. (2013), What caused the long duration of the Paleocene-Eocene Thermal Maximum?, *Paleoceanography*, *26*, 1–13, doi:10.1002/palo.20039.

Zeebe, R., and J. Zachos (2012), Long-term legacy of massive carbon input to the Earth system: Anthropocene versus Eocene, *Philos. Trans. R. Soc. A*, *371*, 1471–2962.

Zeebe, R. E., J. C. Zachos, and G. R. Dickens (2009), Carbon dioxide forcing alone insufficient to explain Palaeocene-Eocene Thermal Maximum warming, *Nat. Geosci.*, *2*(8), 576–580.